Assessing hydrological sampling approaches in the Cape Verde frontal zone in November 2017

Inés Hernández-García [1], Josep Coca [2], Antonio Ramos [3],
Ángel Rodríguez-Santana [1], Francisco Machín [1]

[1] Oceanografía Física y Geofísica Aplicada (OFYGA), IU-ECOAQUA, Universidad de Las Palmas de Gran Canaria, Edificio de Ciencias Básicas, Campus Universitario de Tafira, 35017, Las Palmas de Gran Canaria, Spain.
(IH-G) E-mail: ines.hernandez@ulpgc.es. ORCID iD: https://orcid.org/0000-0002-6217-7835
(AR-S) E-mail angel.santana@ulpgc.es. ORCID iD: http://orcid.org/0000-0003-1960-6777
(FM) (Corresponding author) E-mail: francisco.machin@ulpgc.es. ORCID iD: http://orcid.org/0000-0002-4281-6804

[2] GRAFCAN, Avenida Juan XXIII, 7, Edificio Campo España, 35004, Las Palmas de Gran Canaria, Spain.
(JC) E-mail: jcocsae@grafcan.com. ORCID iD: https://orcid.org/0000-0003-0625-8240

[3] Biodiversidad y Conservación (BIOCON), IU-ECOAQUA, Universidad de Las Palmas de Gran Canaria, Edificio de Ciencias Básicas, Campus Universitario de Tafira, 35017, Las Palmas de Gran Canaria, Spain.
(AR) E-mail: antonio.ramos@ulpgc.es. ORCID iD: http://orcid.org/0000-0003-1374-5805

Summary: The Cape Verde Frontal Zone in the eastern North Atlantic Subtropical Gyre is a complex region where the warmer North Atlantic Central Water interacts with the colder South Atlantic Central Water, forming the Cape Verde Front (CVF) with a sharp thermohaline gradient. The CVF exhibits high variability due to lateral intrusions, upwelling system filaments, and mesoscale and submesoscale eddy fields. In November 2017, the FLUXES project surveyed the CVZ extensively using shipborne conductivity, temperature, and depth (CTD) measurements, a SeaSoar and two deep gliders equipped with biochemical and dynamical instruments. The primary objective of this paper is to intercompare the spatial scales recovered by the different sampling methods in the CVF, incorporating Copernicus numerical model outputs. Wavelet analysis is used for a quantitative assessment of scales resolved by different sampling methods. The results highlight shipborne CTD depth, down to 1500 m, SeaSoar speed, with a 14 h sampling time, and specific capabilities of both the gliders and the SeaSoar in capturing small scales of between 1 and 5 km. The gliders slightly outperformed the SeaSoar in spatial resolution, emphasizing their effectiveness in revealing smaller features in this dynamic zone.

Keywords: water masses, gliders, SeaSoar, numerical models, wavelet analysis, mesoscale.

Análisis de métodos de muestreo hidrológico en la zona frontal de Cabo Verde en noviembre de 2017

Resumen: El Frente de Cabo Verde (CVF), en el Atlántico Norte oriental, es una región compleja donde el Agua Central del Atlántico Norte, más cálida, interactúa con el Agua Central del Atlántico Sur, más fría, formando un marcado gradiente termohalino. El CVF muestra gran variabilidad debido a intrusiones laterales, filamentos del sistema de afloramiento y remolinos a mesoescala y submesoescala. En noviembre de 2017, el proyecto FLUXES realizó un extenso muestreo en el CVF mediante mediciones de Conductividad, Temperatura y Profundidad (CTD) desde un barco, un SeaSoar y dos gliders profundos equipados con instrumentos bioquímicos y dinámicos. Este artículo tiene como objetivo comparar las escalas espaciales detectadas por los diferentes métodos de muestreo en el CVF, incluyendo los resultados del modelo numérico de Copernicus. Se empleó el análisis wavelet para evaluar cuantitativamente las escalas resueltas por cada método. Los resultados destacan la capacidad del CTD para alcanzar profundidades de hasta 1500 m, la rapidez del SeaSoar, con un tiempo de muestreo de 14 horas, y las capacidades específicas tanto del glider como del SeaSoar para captar escalas pequeñas entre 1 y 5 km. El glider supera al SeaSoar en resolución espacial, mostrando su eficacia en la detección de estructuras más pequeñas.

Palabras clave: masas de agua, vehículo submarino autónomo (gliders), vehículo operado remotamente (SeaSoar), modelos numéricos, análisis wavelet, estructuras de mesoescala.

INTRODUCTION

Traditionally, ocean analysis has relied on datasets obtained from ship-based measurements and moorings. In addition, remote-sensing technologies have gained widespread usage and continue to advance. However, current remote-sensing technologies primarily focus on the ocean's surface. Over the past few decades, subsurface floats such as Argo floats, remotely operated vehicles and autonomous underwater vehicles (AUVs) such as gliders have emerged, offering a vast array of applications in oceanography (Bachmayer et al. 2004, 2006, Hernández-García et al. 2018, Ramos et al. 2018).

These state-of-the-art sampling systems now enable access to ocean phenomena across a wide range of scales, from the size of the ocean basin to microscales. They are highly portable and suitable for sampling intermittent and localized phenomena such as upwelling events. Notably, gliders offer relative control over horizontal location, allowing scientists to strategically select where to conduct profiles. Furthermore, gliders boast lower energy consumption than other AUVs, enabling longer and deeper operations. However, gliders are limited in terms of the sensors they can carry, which must be compact and lightweight and have low power consumption (Rudnick et al. 2004, Bachmayer et al. 2004).

The Cape Verde Frontal Zone (CVFZ) is a dynamically complex region situated in the eastern North Atlantic Subtropical Gyre (20°W to 30°W, ~20°N). This front is defined by the strong interleaving of two main water masses at surface and central levels in the North Atlantic Ocean—North Atlantic Central Water (NACW) and South Atlantic Central Water (SACW) (Tomczak 1981, Barton 1987, Pelegrí et al. 2017).

NACW shows an almost linear relationship between temperature and salinity within the range of 11°C to 18.65°C and 35.47 to 36.76, while SACW shows this relationship within the range of 9.7°C to 15.25°C and 35.177 to 35.7. SACW also shows a minimum in oxygen levels, dropping below 1.5 mL L^{-1}, whereas NACW shows low nutrient levels and a high oxygen concentration (Tomczak 1981, Hagen 1985, Zenk et al. 1991). Below these water masses, Antarctic Intermediate Water (AAIW) becomes apparent at intermediate layers, and shows a minimum in both salinity and oxygen. Mediterranean Water, found at depths of 800–1200 m and in the form of meddies, is notably warmer and more saline than AAIW (Zenk et al. 1991, Pérez et al. 2001, Bashmachnikov et al. 2015).

The Cape Verde Front (CVF) is traditionally defined by the intersection of the 36.0 isohaline with the 150 m depth isobath (Barton 1987, Zenk et al. 1991). This front persists throughout the year, experiencing high spatial and temporal variability and extending from 20°W to 30°W, at latitudes between 15°N and 22°N, from Cape Blanc to the Cape Verde Islands (Mittelstaedt 1983, Tomczak and Hughes 1980, Zenk et al. 1991). A compilation of CVF positions from synoptic surveys by Zenk et al. (1991) suggested that spatial variations of the front are at least of the order of 300 km in the region off Cape Blanc.

This highly meandering thermohaline front is marked by the presence of intrusions, filaments from the upwelling system and eddy activity (Martínez-Marrero et al. 2008). The upwelling between 20°N and 25°N exhibits maximum intensity during spring and autumn, featuring sharp gradients in temperature (<3°C) and salinity (<0.08) at depths down to 600 m. The temperature decrease with depth compensates for the salinity decrease, resulting in both variables effectively counterbalancing their effects on density and maintaining the front's dynamic stability. In this highly variable region, high-definition sampling methods prove crucial to capture all the processes observed during sampling (Hughes and Barton 1974, Pérez-Rodríguez et al. 2001, Martínez-Marrero et al. 2008). An unprecedented observational effort was undertaken in the context of the CVF by the FLUXES-II campaign in November 2017, comprehensively sampling the region using both traditional and innovative instruments. The objective of this paper is to present an intercomparison between the in situ FLUXES-II data and Copernicus Mercator model outputs to assess their respective capabilities in capturing the features of this highly variable area.

DATA AND METHODS

FLUXES-II

The FLUXES-II cruise took place in the CVFZ between 2 and 24 November 2017, utilizing the BIO Sarmiento de Gamboa. The primary objective of the FLUXES project was to investigate the hydrographic characteristics of the CVF. The expedition involved various measurements including CTD stations, SeaSoar, glider deployments, ADCP recordings and turbulence measurements (Burgoa et al. 2021, Campanero et al. 2022).

Data Sources

This study focuses on data collected from ship-based CTD stations (referred to as Ship CTD), SeaSoar and gliders, as well as Mercator model outputs (detailed descriptions of each dataset are provided below). The spatial distribution of the data is shown in Figure 1.

Mercator model

The numerical model outputs were sourced from the Copernicus Marine Environment Monitoring Service dataset GLOBAL_ANALYSIS_FORECAST_PHY_001_024. This model, which provides daily outputs, is a numerical forecasting model (von Schuckmann et al. 2016). The dataset utilized for this study corresponds to the model outputs covering the same spatial locations and dates as the glider data. It offers a horizontal resolution of 1/12° (0.083°) and comprises 50 vertical levels spanning from the sea surface to 5500 m depth.
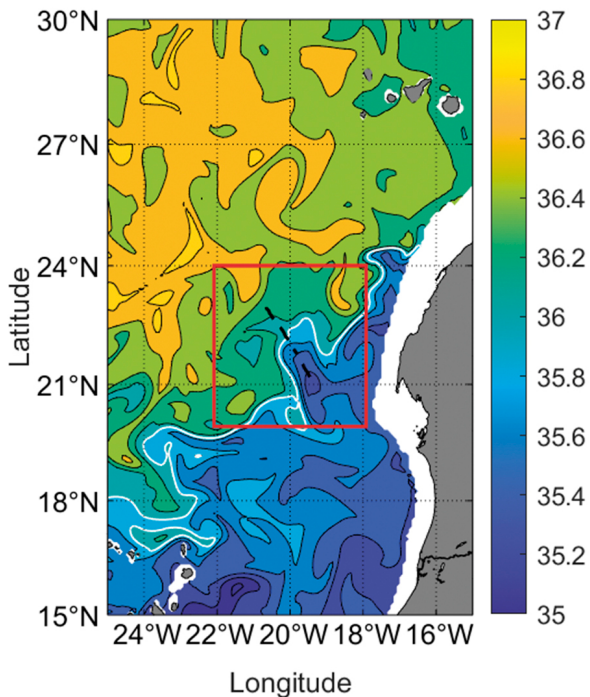
Fig. 1. – Map illustrating the study area for this project. Salinity data at 150 m are depicted, emphasizing the isohaline of 36 with the white contour. The black line represents the transect used for this analysis, corresponding to a portion of the FLUXES-II cruise sampling. The red square highlights the area sampled by the FLUXES-II survey. The map was generated using global Mercator model data on 13 November 2017.

Ship CTD

A total of 48 stations were sampled using the CTD rosette system, with 36 stations being utilized for this study between 10 and 20 November. These measurements encompassed depths from the sea surface down to 1500 m. The stations were approximately 9.26 km apart, with a vertical resolution of about 1 m (Burgoa et al. 2021, Campanero et al. 2022).

SeaSoar

The SeaSoar, a vehicle performing undulations from the surface to a depth of 500 m, was deployed in a continuous towed manner behind the research vessel, yielding high spatial resolution datasets (Pollard 1986, Hales and Takahashi 2002, Allen et al. 2002). For this study, the chosen transect was T5 from the FLUXES-II cruise, conducted on 8 November. This transect sampled the water column from the surface to approximately 400 m depth, with a horizontal resolution of approximately 2.5 km and a vertical resolution of 0.5 m (Burgoa et al. 2021, Campanero et al. 2022).

Gliders

Gliders, categorized as AUVs, dynamically adjust their buoyancy to traverse the water column, utilizing

ocean currents to facilitate their movement (Bachmayer et al. 2006). Two gliders, Bio-584 and Dyna-585, were deployed between 4 and 21 November. These gliders sampled from the surface to 1000 m over a distance exceeding 350 km. Bio-584 was chosen for this study as both gliders provided similar observations. The dataset from Bio-584 has a horizontal spatial resolution of approximately 1 km and a vertical resolution of around 1 m (Burgoa et al. 2021, Campanero et al. 2022).

Sea level and surface velocity from satellite data

Sea level anomaly and the velocity field estimated from satellite observations were obtained from the Copernicus Marine Environment Monitoring Service dataset SEALEVEL_GLO_PHY_L4_REP_OBSERVATIONS_008_047. This dataset integrates sea level anomaly data from different altimeter missions, achieving a horizontal resolution of up to 1/4°.

Data processing

The variables considered in this study encompass potential temperature, practical salinity, potential density and oxygen. Practical salinity from the Ship CTD was calibrated by analysing 51 water samples. Oxygen measurements from the CTD stations were calibrated using in situ samples, ensuring a precision of ±0.53 µmol kg^{-1} (Burgoa et al. 2021). Glider data were processed using the SOCIB Glider Toolbox incorporating thermal lag correction and quality control (Troupin et al. 2015).

The location of the CVF within the depth range of 100 to 650 m was calculated using the methodology described by Burgoa et al. (2021), defining the front location based on salinity values representing a 50% contribution of NACW and SACW.

Wavelet Analysis

The comparison of sampling methods was based on the scales they can effectively capture, allowing for a focused analysis of various processes. We utilized wavelet analysis to objectively quantify the scales accessed by the different sampling methods. Wavelet analysis is a technique that decomposes a time series into a time-frequency space, aiding in the determination of the primary frequencies of the signal. It provides a clear visual representation of the signals, presenting local values for the amplitude and phase for each harmonic of a dataset. Thus, wavelets are highly valuable for describing nonstationary processes that cannot be adequately detected using classical Fourier transform techniques. Furthermore, wavelet analysis can be applied to signals of any size, whereas Fourier transform requires a predetermined size (Combes et al. 1990, Lau and Weng 1995, Torrence and Compo 1998).

Wavelet analysis was pioneered by Morlet et al. (1982), Morlet (1983) and Grossmann and Morlet (1984). It has found extensive use in climatic studies, climatic time series analysis (Kumar and Foufou-

la-Georgiou 1993, Gao and Li 1993, Collineau and Brunet 1993, Gollmer et al. 1995, Gu and Philander 1995, Lau and Weng 1995, Mak 1995, Wang and Wang 1996, Baliunas et al. 1997, Torrence and Compo 1998, Moron et al. 1998, Yiou et al. 2000, Jevrejeva et al. 2003, Grinsted et al. 2004, Venkata-Ramana et al. 2013), various ocean processes (Farge 1992, Meyers et al. 1993, Gamage and Blumen 1993, Gamage and Hagelberg 1993, Liu 1994, Weng and Lau 1994, Camayo and Campos 2006, Garel et al. 2016), medical research, seismic signals, image processing, and more (Torrence and Compo 1998).

In this study, we utilized the complex continuous Morlet wavelet method. A complex wavelet enables the detection of both amplitude and phase. Continuous wavelets are particularly useful for scale analysis, although they can be redundant on larger scales (Lau and Weng 1995, Torrence and Compo 1998). The wavelet analysis was applied to all the different data sources: Mercator model outputs, Ship CTD, SeaSoar and gliders. After characterizing the primary features within the domain, we proceeded to analyse the scales captured by various sampling methods. The wavelet analysis was conducted at specific depths within the central water region: 150, 350, and 600 m (note that the SeaSoar did not sample beyond 400 m). The salinity variable was chosen for the wavelet analyses at these depths because of its well-defined signature of the frontal zone. The depth of 150 m holds significance, traditionally defining the CVF by the 36.0 isohaline at this depth (Zenk et al. 1991). The data series were obtained within the same latitudinal range spanning approximately 200 km, with the assumption that the identified features should remain consistent across the CVF, regardless of the observation methodology. The figures are presented in a NW to SE orientation.

The horizontal resolution for each sampling method, calculated as the mean distance between two consecutive profiles, is detailed in Table 1. Amplitudes smaller than the Nyquist frequency, which is twice the horizontal spatial resolution for each method, were excluded from the analysis.

Table 1. – Spatial and temporal resolution of the sampling methods and the numerical model.

Sampling method	Horizontal spatial resolution (km)	Vertical range (m)	Sampling period (days)
Mercator model	11.5	1	17
Ship CTD	9.3	1	5
SeaSoar	2.5	0.5	1
Glider	0.9	1	17

RESULTS

TS diagram and water masses

Figures 2A and 2B depict the TS diagram obtained along the transect using the glider. The primary water masses identified were NACW and SACW. SACW was slightly less saline and colder than the NACW at equivalent depths. The surface data exhibited the highest variability, attributable to insolation during the summer and autumn, as well as the potential influence of water exported in filaments from the African upwelling system. Some mixed AAIW was observed at intermediate depths (deeper than 800 m).

The majority of the data points correspond to NACW, as evidenced by the TS frequency diagram in Figure 2B. The TS diagrams obtained through the
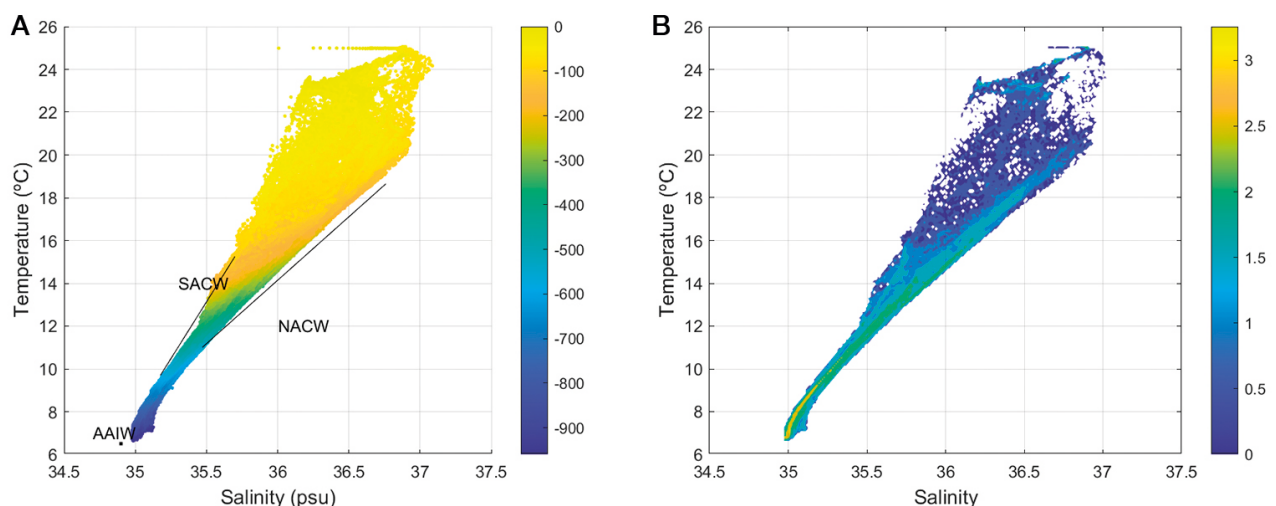

Fig. 2. – A, TS diagram obtained from the glider; and B, frequency distribution of each TS cell for the glider data. Reference lines for SACW and NACW are adopted from Tomczak (1981). The AAIW point is sourced from Pérez et al. (2001). Dots are colour-coded based on their depth in metres in A and logarithm of the frequency in B.
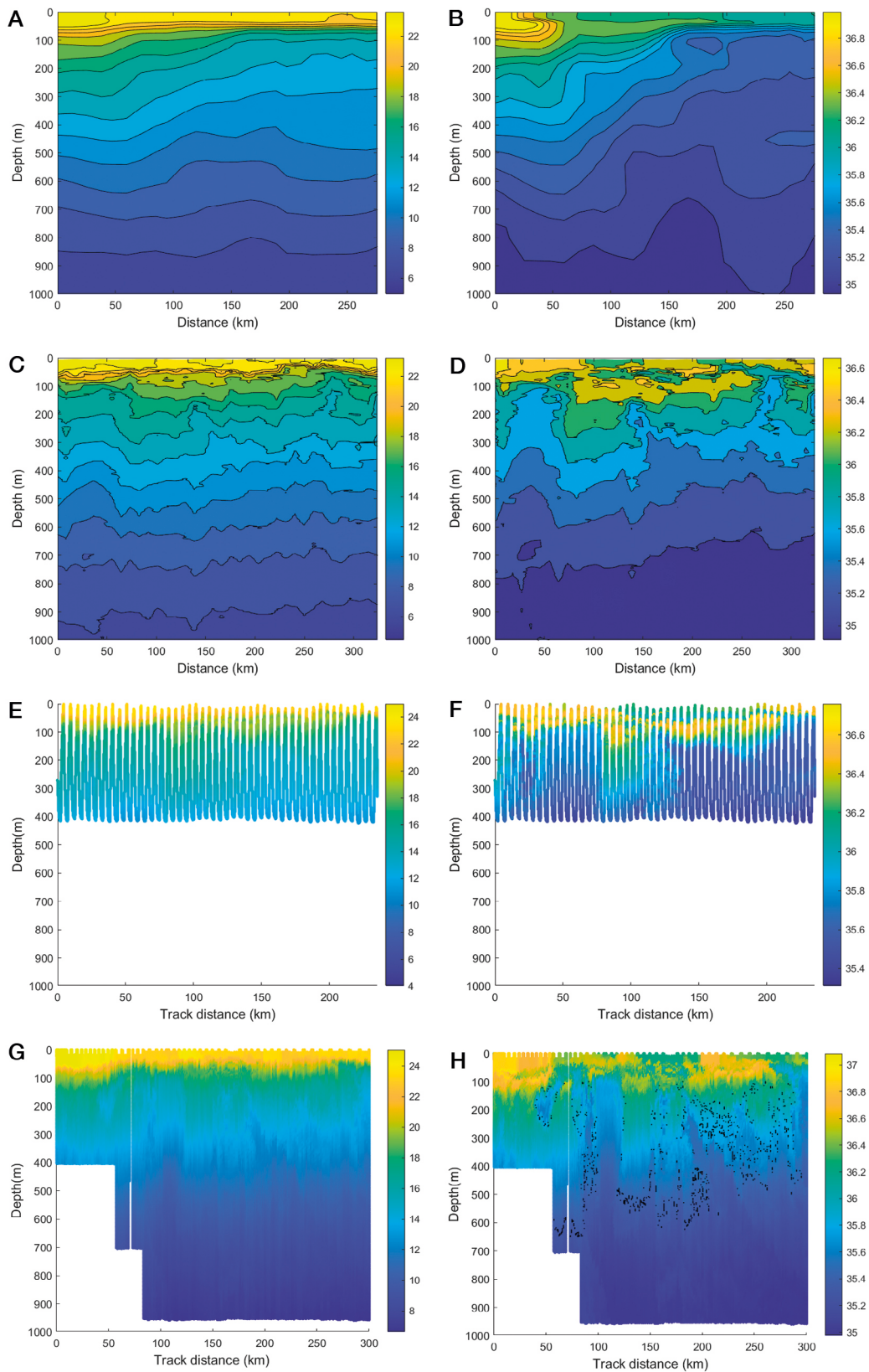
Fig. 3. – Vertical section of (A, D, E, G) potential temperature and (B, D, F, H) salinity obtained by the Mercator model, Ship CTD, SeaSoar and glider along the track. The orientation is from north (left) to south (right). The black dots indicate the position of the Cape Verde Front between 100 and 650 m according to Burgoa et al. (2021).

different sampling methods in this study exhibit consistent patterns.

Vertical sections

Mercator model

The model outputs were extracted based on the latitude and longitude range provided by the glider, as well as its temporal range, starting from the north on 4 November and ending in the south on 21 November. The model provides data down to 5500 m depth, but for this analysis we used data down to 1000 m.

The temperature ranged from 5°C to 24.8°C and the salinity from 34.9 to 37.1 (Fig. 3A, B). The water column appeared stratified based on the temperature. The salinity distribution exhibited more variability than the temperature. In the first half of the track, there was more saline water in the surface layer, while the temperature remained relatively constant in this layer throughout the sampling.

Ship CTD

The ship performed 36 stations from 20.5°N to almost 23°N, with a separation of 9.5 km. The observations started on 11 November and concluded on 16 November, reaching depths down to 1500 m, although for this analysis we used data down to 1000 m.

The temperature ranged from 4.5°C to 24.5°C, and the salinity from 34.9 to 36.9 (Fig. 3C, D). The temperature and salinity distributions showed intrusions of SACW, which is colder and less salty than NACW, at depths ranging from 100 to 500 m. These intrusions were found at approximately 50 and 150–200 km. Notably, the second intrusion appeared to be tilted.

The last 75 km (>200 km), at the lowest latitude, showed more saline water in the surface layer. The temperature in the surface layer was similar along the whole track.

SeaSoar

For this study, we utilized the transect T5 from the SeaSoar grid. It began in the north and proceeded southward, as did all the other sampling methods, from 8 to 9 November. The SeaSoar sampled down to a depth of 400 m.

The temperature ranged from 10.8°C to 23.7°C and the salinity from 35.3 to 36.7 (Fig. 3E, F). In the surface layer, the water was warmer and saltier along the first 75 km than within the rest of the track.

The vertical sections revealed three intrusions of SACW, occurring between 25 and 75 km, 125 and 175 km, and >200 km. These intrusions began at a depth of 100 m and extended to the SeaSoar's maximum depth.

Glider

The glider initiated its southward track at 23°N and continued until 21°N. It continuously dived from the surface down to a depth of 1000 m between November 4th and November 21st.

The temperature ranged from 6.6°C to 25.1°C and the salinity from 34.9 to 37 (Fig. 3G, H). High temperatures were observed within the surface layer (<100 m) along the entire section.

The vertical sections displayed three large intrusions of SACW, occurring between 75 and 125 km, 175 and 225 km, and >275 km. The second intrusion was noticeably tilted to the north. The intrusions were captured in greater detail than in the CTD and SeaSoar observations and seemed to be located between 100 and 800 m depth.

The location of the CVF is indicated following the methodology developed by Burgoa et al. (2021), highlighting the limits between NACW and SACW.

The density distribution exhibited a relatively flat pattern along the entire section, as expected for a density-compensated front (Fig. 4A). The density ranged from 1024.1 to 1031.8 kg m^{-3}.

The oxygen distribution (Fig. 4B) displayed the same intrusions as the salinity and temperature distributions. The SACW intrusions were marked by a lower value of oxygen concentration. In the surface layer, the oxygen concentration remained high throughout the entire track. The oxygen concentration ranged from 26.8 to 227.8 µmol L^{-1}.

Wavelet analysis of in situ signals

Analysis performed at 150 m

At this depth, salinity fluctuated between 35.4 and 36.6 (Fig. 5). The Mercator model sampling exhibited a smooth, slightly decreasing trend. Conversely, the Ship CTD data showed variability without a clear trend, showcasing a sharp decrease at both edges with higher values at the centre of the track. In the SeaSoar sampling, a slight decreasing trend was observed, with an increase in salinity in the middle of the track (22°N) followed by a decrease. The SeaSoar sampling also showed higher-frequency variability than the Mercator model and the Ship CTD. The glider sampling, on the other hand, showed the highest variability, with no clear decreasing or increasing trend; a relative maximum salinity was sampled at the middle of the track (22°N-21°N). It is important to note that the position of the front varied among the different sampling methods because of the highly variable dynamics of the front and the fact that the system was sampled at different moments.

The wavelet analysis revealed that the numerical model captured scales within a relatively narrow band ranging from 23 to 64 km (Fig. 6A, Table 2). However, these scales were not constant along the entire track, and no significant scales were identified.
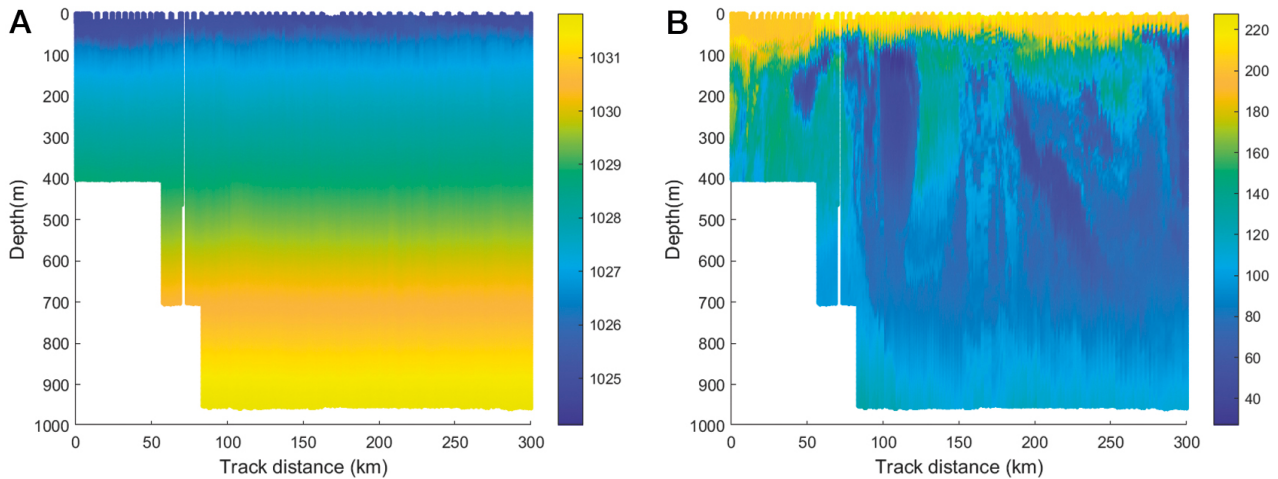
Fig. 4. – Vertical section of (A) density (kg m⁻³) and (B) dissolved oxygen concentration (µmol L⁻¹) obtained by the glider along its track. The orientation is from north (left) to south (right).

than the range at 150 m (Fig. 7). A decreasing trend was observed in the salinity series as they approach the African coast. The model sampling showed lower salinity in the middle of the track and higher salinity at the edges, with a smooth spatial distribution. The Ship CTD showed a salinity distribution consistent with various signatures as the track crosses the front, showcasing salinity increases at 22.4°N, 21.3°N, and 20.8°N, as well as several decreases at 21.6°N, 21.1°N, and 20.5°N. Both SeaSoar and the glider showed the highest variability: SeaSoar showed a decreasing trend, also marked by several sharp changes related to the sampling of the front, while the glider showed abrupt changes at various points during its southward track, capturing a high-frequency spatial variability throughout the entire path.
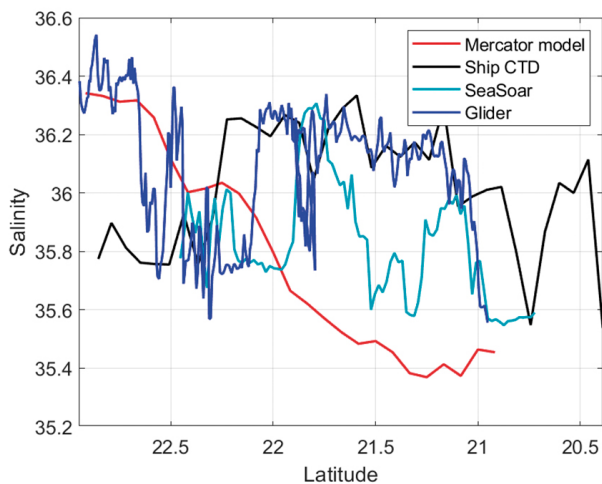
Table 2. – Range of scales (km) captured by each method at each depth.

Depth	Mercator model	Ship CTD	SeaSoar	Glider
150 m	23–64	18.6–128	5–64	1.8–128
350 m	23–64	18.6–128	5–64	1.8–128
600 m	48–64	18.6–128	-	1.8–128

The Ship CTD captured scales within a wider range of 18.6 to 128 km (Fig. 6B). The range was slightly narrower at the beginning of the signal, broadening towards the end of the path covered, capturing smaller scales. A significant scale was identified at around 32 km towards the end of the track.

The SeaSoar captured scales within the range of 5 to 64 km (Fig. 6C). However, scales smaller than 16 km appeared intermittently along the track. The scale of 32-64 km was significant in the middle of the track.

The glider sampling captured scales in the widest range, spanning from 1.8 to 128 km (Fig. 6D). Scales smaller than 8 km were not constant during the track. Significant scales around 2-4 km and at 32 km were identified at some points in the first third of the track. Additionally, a significant scale of 64 km was obtained at the beginning and in the middle of the track.

In summary, at this depth the glider captured the smallest scales and recovered the widest range, while the model and the Ship CTD recovered the narrowest range. The glider, followed by both the SeaSoar and Ship CTD, exhibited the highest number of significant scales and the highest spatial variability.

Analysis performed at 350 m

The salinity signal at 350 m showed values ranging from 35.2 to 36, which is lower and slightly narrower

Fig. 5. – Salinity series from the Mercator model, Ship CTD, SeaSoar and glider at 150 m, starting at the NW (left) and finishing at the SE (right).
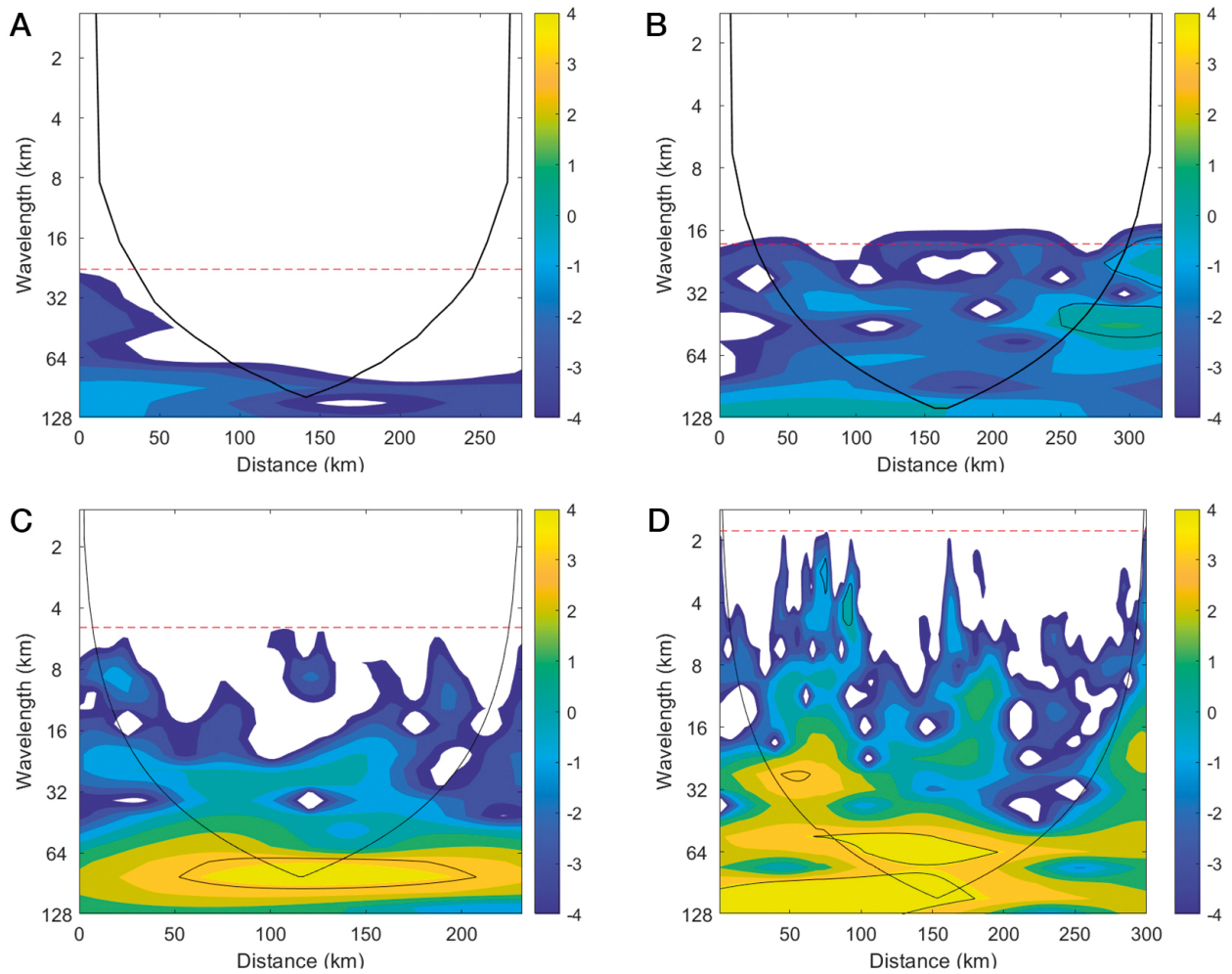
Fig. 6. – Wavelet analysis from the model (A), Ship CTD (B), SeaSoar (C) and glider (D) salinity at 150 m. The wavelet results on the area under the black line may be affected by edge effects and are not considered as valid. The red dotted line indicates the minimum accepted wavelength, 2*horizontal resolution (the horizontal Nyquist frequency). The black contour indicates the significant results. The Y and Z axis are logarithmic. The Z values represent the base 2 logarithm of the wavelet power spectrum. The signals start at the NW (left) and finish at the SE (right). A, Mercator; B, ship CTD; C, SeaSoar; D, glider.
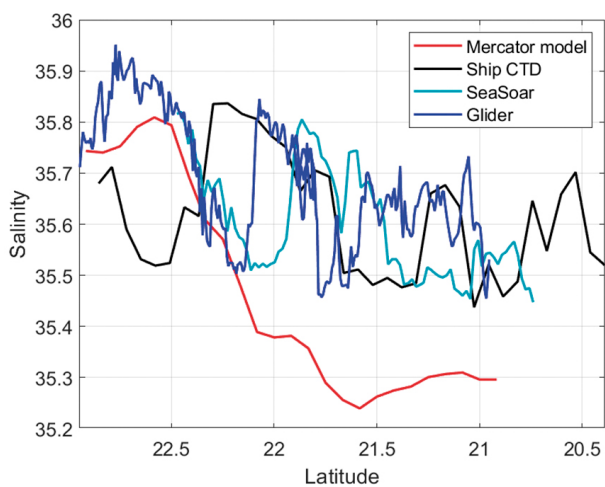
Fig. 7. – Salinity series from the Mercator model, Ship CTD, SeaSoar and glider at 350 m, starting at the NW (left) and finishing at the SE (right).

The Mercator model captured scales ranging from 23 to 64 km at the NW end, and around 64 km on the rest of the path (Fig. 8A, Table 2), yet no significant scales were identified. The smaller scales were absent in the second half of the track.

The Ship CTD displayed scales between 18.6 and 128 km (Fig. 8B). The range broadened slightly towards the end of the track for smaller scales. However, scales smaller than 64 km were not consistently present. A significant scale was observed in the 16–32 km range at the end of the signal.

The SeaSoar captured scales between 5 and 64 km (Fig. 8C). The range remained constant throughout the signal, but scales smaller than 32 km appeared intermittently. The analysis did not reveal any significant scales.

The glider exhibited the widest range of scales, spanning from 1.8 to 128 km (Fig. 8D). Towards the final segment of the transect (>200 km), the range narrowed down to 4–128 km. A significant scale was ev-
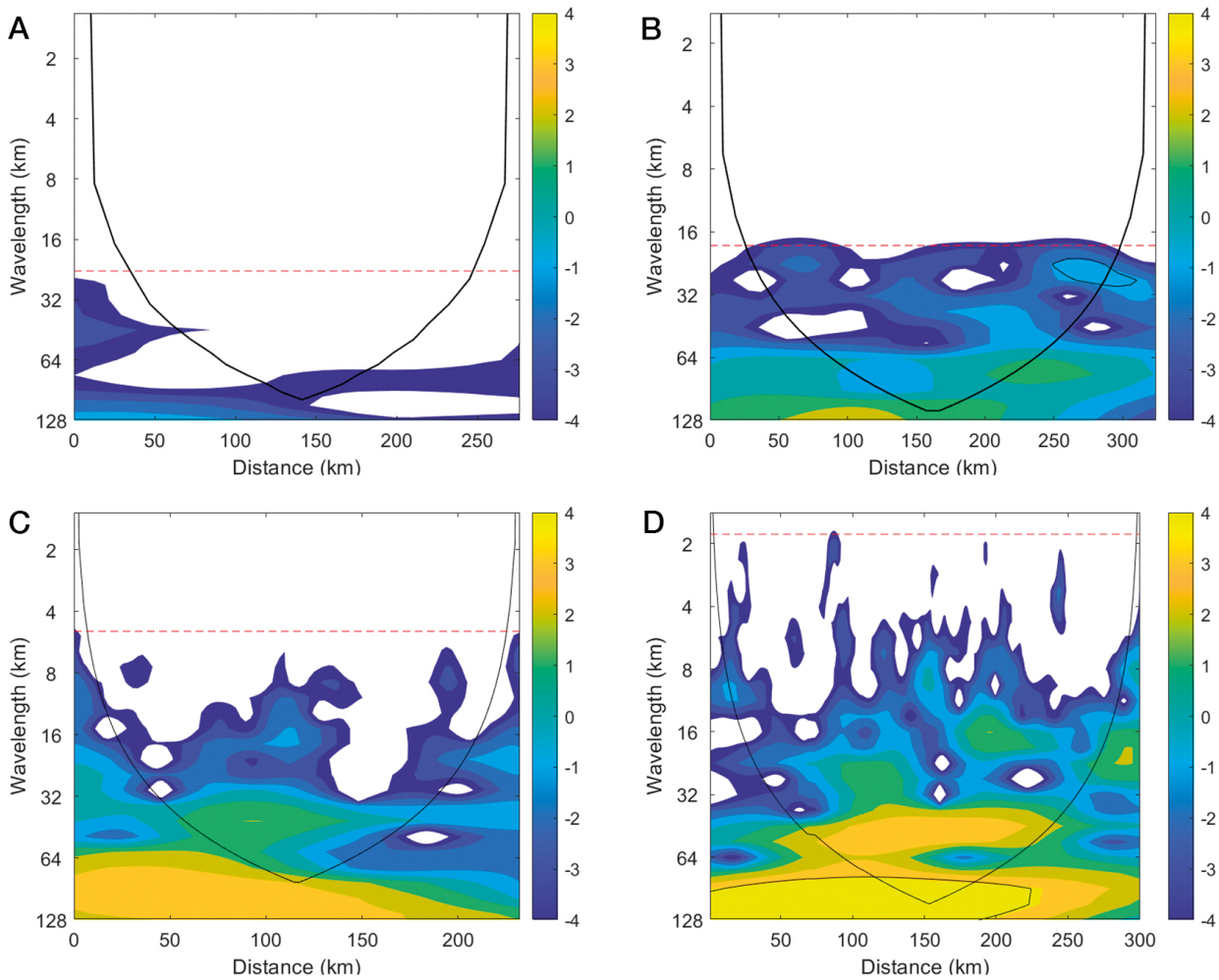
Fig. 8. – Wavelet analysis from the model (A), Ship CTD (B), SeaSoar (C) and glider (D) salinity at 350 m. The wavelet results on the area under the black line may be affected by edge effects and are not considered as valid. The red dotted line indicates the minimum accepted wavelength, 2*horizontal resolution (the horizontal Nyquist frequency). The black contour indicates the significant results. The Y and Z axis are logarithmic. The Z values represent the base 2 logarithm of the wavelet power spectrum. The signals start at the NW (left) and finish at the SE (right). A, Mercator; B, ship CTD; C, SeaSoar; D, glider.

ident in the 96–128 km range for the second third of the track.

Consistent with the results at 150 m, the glider showed the widest range and captured the smallest scales, while the model and the Ship CTD showed the narrowest range. Notably, only the glider and the Ship CTD showed significant scales.

Analysis performed at 600 m

The salinity at 600 m showed a narrower range, falling between 35 and 35.4 (Fig. 9). A consistent decreasing trend was observed across all sampling methods. The model's sampling reflected the lowest salinity levels, particularly at the track's centre. The Ship CTD showed a variability greater than that of the model, while the glider showed the highest variability.

The results from the analysis at 600 m indicate that the Mercator model's sampling captured scales be-
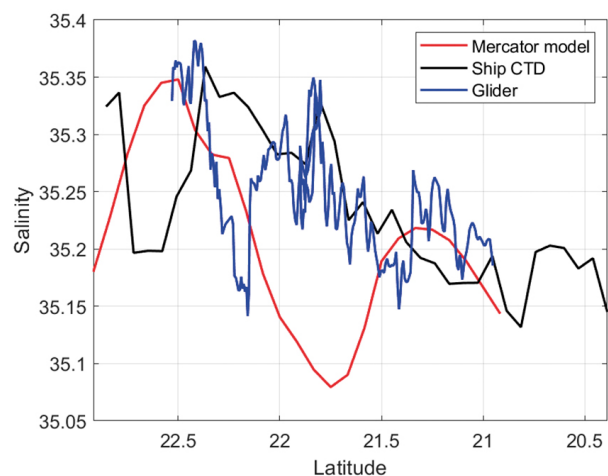

Fig. 9. – Salinity series from the Mercator model, Ship CTD and glider at 600 m, starting at the NW (left) and finishing at the SE (right)
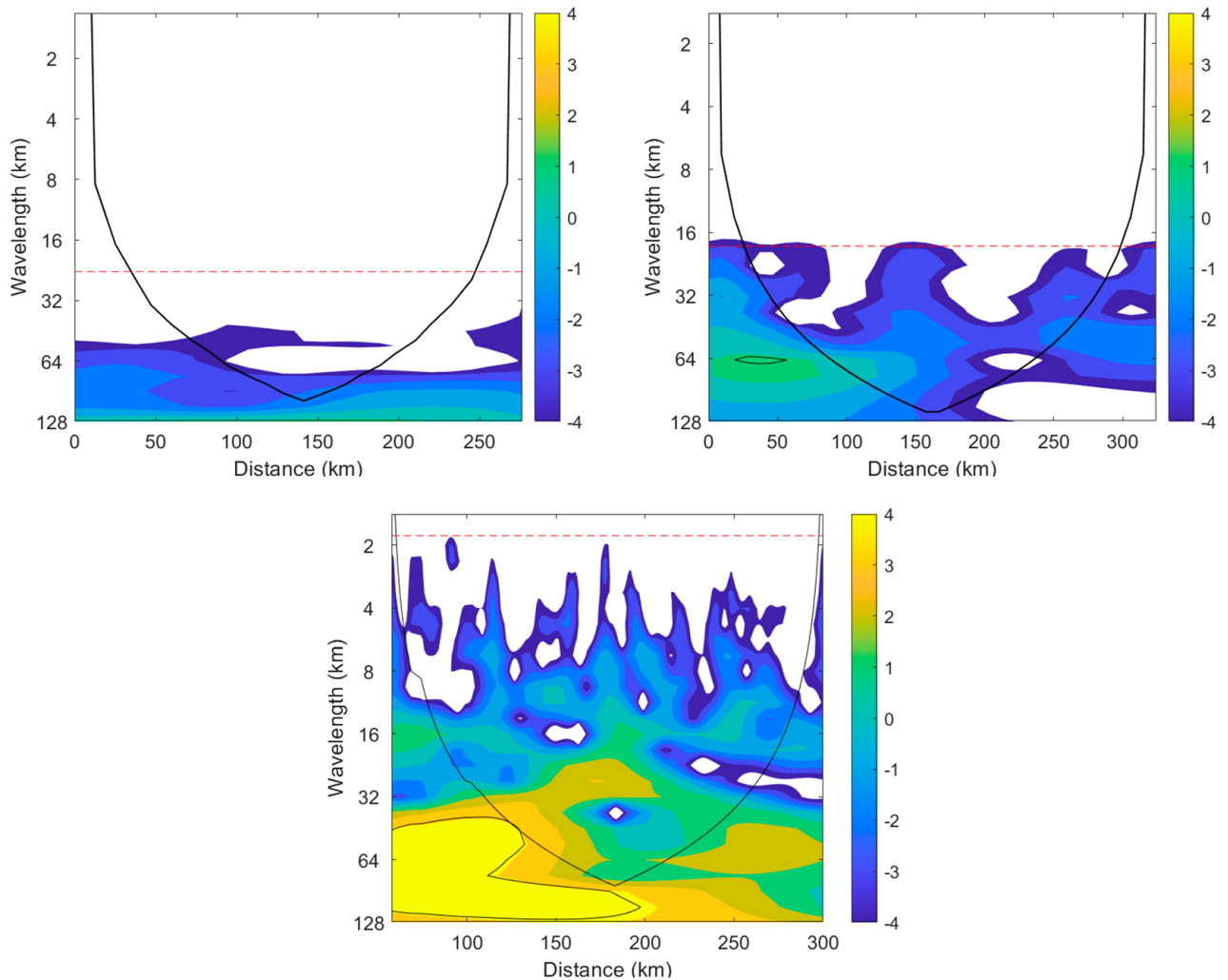
Fig. 10. – Wavelet analysis from the model (A), Ship CTD (B) and glider (C) salinity at 600 m. The wavelet results on the area under the black line may be affected by edge effects and are not considered as valid. The red dotted line indicates the minimum accepted wavelength, 2*horizontal resolution (the horizontal Nyquist frequency). The black contour indicates the significant results. The Y and Z axis are logarithmic. The Z values represent the base 2 logarithm of the wavelet power spectrum. The signals start at the NW (left) and finish at the SE (right). A, Mercator; B, ship CTD; C, glider.

tween 48 and 64 km, without yielding any significant scales (Fig. 10A, Table 2).

The Ship CTD captured scales ranging from 18.6 to 128 km (Fig. 10B). However, the scales smaller than 32 km were not consistently present throughout the signal, and the scales greater than 64 km disappeared towards the end of the track. No significant scales were obtained.

The glider exhibited the widest band of scales, spanning between 1.8 and 128 km (Fig. 10C). The scales smaller than 16 km appeared intermittently. However, no significant scales were captured.

The range of scales captured by the Mercator model was narrower at 600 m than at 150 and 350 m. Conversely, the glider and Ship CTD showed a similar scale range to the other depths. No significant scales were captured at this depth. As observed previously, the glider captured the broadest range of scales and

showed the highest spatial variability, while the Mercator model's sampling showed the narrowest range of scales.

DISCUSSION AND CONCLUSIONS

The intercomparison between the various sampling strategies shed light on the distinct characteristics of the vertical sections produced. Notably, the vertical sections of the model dataset lacked clear features, in contrast to the CTD, SeaSoar and glider data, which showed similar oceanographic structures. This result for the model might be improved using a higher resolution. Specifically, the Ship CTD results appeared coarsest in resolution, whereas the glider data offered the most detailed insights. A consistent finding across these methods was the stronger variability in the surface layer, attributed to atmospheric
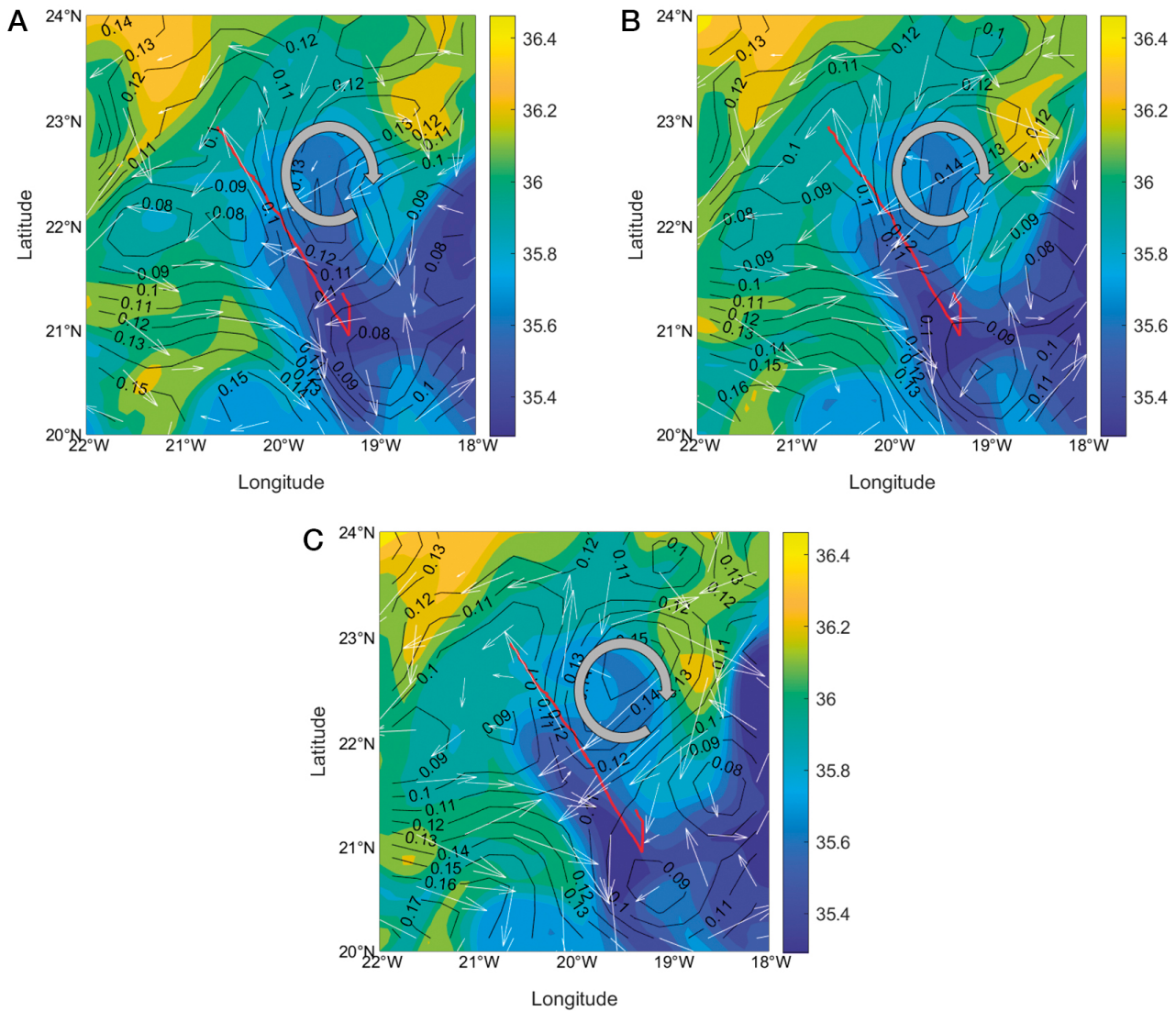
Fig. 11. Temporal evolution of the eddy found during the sampling on (A) 13 November, (B) 17 November and (C) 21 November. The salinity data (coloured map) are taken from the Mercator model, at 222.5 m depth. The SLA data (m), represented by the black contours, and the velocity field (m s⁻¹), represented by the white arrows, are taken from satellite data. The big grey curved arrow indicates the location of the eddy. The red line indicates the path of the glider. A, November 13; B, November 17; C, November 21.

interaction and upwelling filaments. Additionally, a significant feature was the lateral intrusion of SACW into NACW.

Previous studies on the CVF have reported analogous structures. For instance, Barton (1987) identified an anticyclonic eddy with a diameter of approximately 20 km in the CVF. They also noted meandering patterns of around 200 km at the front, although a direct comparison to our results is limited by the length of our sampling track. Similarly, Koshlyakov and Grachev (1973) found an anticyclonic eddy at 16°N, 33°W with a diameter ranging from 90 to 200 km, aligning with the spatial scales captured in our wavelet analysis.

In terms of sampling speed, the SeaSoar emerged as the fastest method, with a 14 h sampling, providing a close approximation to a synoptic view. Converse-

ly, the glider, being the slowest in sampling, with a 17 days duration, potentially sacrificed some synopticity. Rudnick et al. (2004) emphasized the importance of considering the sampling velocity concerning the timescales of oceanic structures. They cautioned that, due to their slower sampling rate, glider data might inadvertently present temporal variability as spatial structure, challenging the perception of a glider section as a precise snapshot of oceanic conditions. Furthermore, the Ship CTD achieved the greatest sampling depth of all methods, while the SeaSoar achieved a shallower sampling depth.

The complexity of the CVF, as evidenced in our results, requries swift sampling methods with high vertical and horizontal resolutions to attain an accurate and comprehensive portrayal. Key considerations in-

clude vertical and horizontal resolution, temporal synopticity and sampling independence. In this context, the glider stood out because of its independence from the ship, enabling diverse sampling paths if required. However, the challenge with ship-based methods lies in their availability, particularly given the time-sensitive nature of sampling certain oceanographic structures. The Ship CTD and SeaSoar typically require dedicated oceanographic cruises, while gliders offer a more flexible deployment and retrieval approach. These considerations underscore the importance of strategically selecting and integrating sampling methods to effectively capture the smaller-scale dynamics of oceanic fronts like the CVF.

The prominent feature of the tilted intrusion of SACW into NACW and its formation mechanism stand out as noteworthy contributions from this sampling endeavour. This intriguing tilted intrusion appears at greater depths than the vertical intrusions, hinting at its possible origin as a vertical intrusion subsequently tilted by external forces. In Figure 11, an amalgamation of data from various datasets, including the Mercator model, SLA and surface velocity from satellite altimetry on three distinct dates, provides a glimpse into the temporal evolution at the CVF, precisely where the tilted intrusion was identified. A dynamic signature emerges, unveiling the presence of an anticyclonic eddy previously characterized by Navarro et al. (2018) that is evident in both SLA and resulting surface velocities. This anticyclonic eddy could induce a baroclinic behaviour, resulting in varying velocities near the surface versus higher depths, generating an along-depth variable drag. This, in turn, could distort a vertical front, ultimately giving rise to a tilted intrusion. Notably, relying solely on data from Ship CTD or SeaSoar might overlook this tilted intrusion. The interpretation of this phenomenon as a coherent oceanographic structure necessitates high-rate spatial sampling.

Finally, the wavelet analysis has proven instrumental in comparing the achieved resolution and the scales each method can capture, aiding in determining the most suitable method aligned with the scientific objective. The amplitude of the scales recovered by the various sampling strategies shows considerable variability, with the glider showing the widest range and the numerical model the narrowest range across all three selected depths. Additionally, the model's wavelet results fell significantly below the spatial Nyquist frequency, distinguishing it from the other sampling methods. At 150 m and 350 m depths, significant signals of approximately 20–25 km were obtained for the Ship CTD in the vicinity of the upwelling, likely associated with lateral intrusions across the front. Furthermore, the SeaSoar and glider data exhibited significant signals at 150 m exceeding approximately 60–80 km in the central domain, likely linked to the meandering of the front. However, no significant signals were obtained at 600 m depth.

The detailed dynamics of the CVF, involving a myriad of processes interacting at various spatial and temporal scales, render this domain an ideal laboratory for conducting intercomparison analyses between different sampling instruments. Additionally, the contrast between the two main water masses might be an advantage to depict the structures more clearly on this analysis. This endeavour effectively unveils the strengths and limitations of these instruments, enriching our understanding of the CVF's complexity.

DATA AVAILABILITY

ACKNOWLEDGEMENTS

FUNDING SOURCES

AUTORSHIP CONTRIBUTION STATEMENT

Inés Hernández-García: Conceptualization, Data curation, Formal analysis, Methodology, Software, Validation, Visualization, Writing – original draft, Writing – review & editing. Josep Coca: Conceptualization, Data curation, Formal analysis, Investigation, Methodology, Software, Resources, Supervision, Validation, Visualization, Writing – original draft. Antonio Ramos: Conceptualization, Formal analysis, Funding acquisition, Investigation, Project administration, Resources, Supervision, Validation, Writing – original draft. Ángel Rodríguez-Santana: Conceptualization, Formal analysis, Funding acquisition, Investigation, Project administration, Resources, Supervision, Validation, Writing – original draft. Francisco Machín: Conceptualization, Data curation, Formal analysis, Investigation, Methodology, Software, Resources, Supervision, Validation, Visualization, Writing – original draft, Writing – review & editing

REFERENCES

Allen J., Cornell J., Moore M., et al. 2002. Operational oceanography using the 'new' SeaSoar ocean undulator. Sea Technol. 43: 35-40.

Bachmayer R., Leonard N.E., Graver J., et al. 2004. Underwater gliders: recent developments and future applications. In: Proceedings of the 2004 International Symposium on Underwater Technology (IEEE Cat. No.04EX869). IEEE, Taipei, Taiwan, pp. 195-200.
https://doi.org/10.1109/UT.2004.1405540

Bachmayer R., Young B.D., Williams C., et al. 2006. Development and deployment of ocean gliders on the Newfoundland Shelf. In: Proceedings of the Unmanned Vehicle Systems Canada Conference 2006. Montebello, Québec.

Baliunas S., Frick P., Sokoloff D., et al. 1997. Time scales and trends in the central England temperature data (1659-1990): A wavelet analysis. Geophys. Res. Lett. 24: 1351-1354.
https://doi.org/10.1029/97GL01184

Barton E.D. 1987. Meanders, eddies and intrusions in the thermohaline front off North-west Africa. Oceanol. Acta. 10: 267-283.

Bashmachnikov I., Nascimento A., Neves F., et al. 2015. Distribution of intermediate water masses in the subtropical northeast Atlantic. Ocean Sci. 11: 803-827.
https://doi.org/10.5194/os-11-803-2015

Burgoa N., Machín F., Rodríguez-Santana A., et al. 2021. Cape Verde Frontal Zone in summer 2017: lateral transports of mass, dissolved oxygen and inorganic nutrients. Ocean Sci. 17: 769-788.
https://doi.org/10.5194/os-17-769-2021

Camayo R., Campos E.J.D. 2006. Application of wavelet transform in the study of coastal trapped waves off the west coast of South America. Geophys. Res. Lett. 33: L22601.
https://doi.org/10.1029/2006GL026395

Campanero R., Burgoa N., Fernández-Castro B., et al. 2022. High-resolution variability of dissolved and suspended organic matter in the Cape Verde Frontal Zone. Front. Mar. Sci. 9: 1006432.
https://doi.org/10.3389/fmars.2022.1006432

Collineau S., Brunet Y. 1993. Detection of turbulent coherent motions in a forest canopy part I: Wavelet analysis. Boundary-Layer Meteorol. 65: 357-379.
https://doi.org/10.1007/BF00707033

Combes J.M., Grossmann A., Tchamitchian P. 1990. Wavelets: Time-Frequency Methods and Phase Space. Proceedings of the International Conference, Marseille, France, December 14-18, 1987. Springer Berlin Heidelberg, Berlin, Heidelberg., 331 pp.
https://doi.org/10.1007/978-3-642-75988-8

Farge M. 1992. Wavelet transforms and their applications to turbulence. Annu. Rev. Fluid Mech. 24: 395-457.
https://doi.org/10.1146/annurev.fluid.24.1.395

Gamage N., Blumen W. 1993. Comparative analysis of low-level cold fronts: Wavelet, Fourier, and empirical orthogonal function decompositions. Mon. Weather Rev. 121: 2867-2878.
https://doi.org/10.1175/1520-0493(1993)121<2867:CAOLLC>2.0.CO;2

Gamage N., Hagelberg C. 1993. Detection and analysis of microfronts and associated coherent events using localized transforms. J. Atmos. Sci. 50: 750–756.
https://doi.org/10.1175/1520-0469(1993)050<0750:DAAMA>2.0.CO;2

Gao W., Li B.L. 1993. Wavelet Analysis of Coherent Structures at the Atmosphere-Forest Interface. J. Appl. Meteor. Climatol. 32: 1717–1725.
https://doi.org/10.1175/1520-0450(1993)032<1717:WAOCSA>2.0.CO;2

Garel E., Laiz I., Drago T., et al. 2016. Characterisation of coastal counter-currents on the inner shelf of the Gulf of Cadiz. J. Mar. Syst. 155: 19-34.
https://doi.org/10.1016/j.jmarsys.2015.11.001

Gollmer S.M., Harshvardhan, Cahalan R.F., et al. 1995. Windowed and Wavelet Analysis of Marine Stratocumulus Cloud Inhomogeneity. J. Atmos. Sci. 52: 3013–3030.
https://doi.org/10.1175/1520-0469(1995)052<3013:WAWAOM>2.0.CO;2

Grinsted A., Moore J.C., Jevrejeva S. 2004. Application of the cross wavelet transform and wavelet coherence to geophysical time series. Nonlinear Processes Geophys. 11: 561-566.
https://doi.org/10.5194/npg-11-561-2004

Grossmann A., Morlet J. 1984. Decomposition of Hardy Functions into Square Integrable Wavelets of Constant Shape. SIAM J. Math. Anal. 15: 723-736.
https://doi.org/10.1137/0515056

Gu D., Philander S.G.H. 1995. Secular Changes of Annual and Interannual Variability in the Tropics during the Past Century. J. Clim. 8: 864–876.
https://doi.org/10.1175/1520-0442(1995)008<0864:SCOAAI>2.0.CO;2

Hagen E. 1985. A meandering intermediate front North-West off Cape Verde Islands. Oceanogr. Trop. 20: 71-83.

Hales B., Takahashi T. 2002. The pumping SeaSoar: a high-resolution seawater sampling platform. J. Atmos. Oceanic. Technol. 19: 1096-1104.
https://doi.org/10.1175/1520-0426(2002)019<1096:TPSAHR>2.0.CO;2

Hernández-García I., Ramos A., Rodríguez-Santana A. 2018. Validation of ocean forecasting model data with those obtained from the first transoceanic autonomous underwater vehicles (gliders) missions in the North-East Atlantic basin. Final degree project, Universidad de Las Palmas de Gran Canaria, 38 pp.

Hughes P., Barton E.D. 1974. Stratification and water mass structure in the upwelling area off northwest Africa in April/May 1969. Deep-Sea Res. Oceanogr. Abstr. 21: 611-620.
https://doi.org/10.1016/0011-7471(74)90046-1

Jevrejeva S., Moore J.C., Grinsted A. 2003. Influence of the Arctic Oscillation and El Niño-Southern Oscillation (ENSO) on ice conditions in the Baltic Sea: The wavelet approach. J. Geohys. Res., D. 108: 4677.
https://doi.org/10.1029/2003JD003417

Koshlyakov M.N., Grachev Y.M. 1973. Meso-scale currents at a hydrophysical polygon in the tropical Atlantic. Deep-Sea Res. Oceanogr Abstr. 20: 507-526.
https://doi.org/10.1016/0011-7471(73)90075-2

Kumar P., Foufoula-Georgiou E. 1993. A New Look at Rainfall Fluctuations and Scaling Properties of Spatial Rainfall Using Orthogonal Wavelets. J. Appl. Meteor. Climatol. 32: 209–222.
https://doi.org/10.1175/1520-0450(1993)032<0209:ANLARF>2.0.CO;2

Lau K.M., Weng H. 1995. Climate Signal Detection Using Wavelet Transform: How to Make a Time Series Sing. Bull. Am. Meteorol. Soc. 76: 2391–2402.
https://doi.org/10.1175/1520-0477(1995)076<2391:CSDUWT>2.0.CO;2

Liu P.C. 1994. Wavelet Spectrum Analysis and Ocean Wind Waves. In: Foufoula-Georgiou E., Kumar P. (eds), Wavelet Analysis and Its Applications. Academic Press, 4: 151-166
https://doi.org/10.1016/B978-0-08-052087-2.50012-8

Mak M. 1995. Orthogonal wavelet analysis: interannual variability in the surface temperature. Bull. Am. Meteorol. Soc. 76: 2391-2402.
https://doi.org/10.1175/1520-0477(1995)076<2179:OWAIVI>2.0.CO;2

Martínez-Marrero A., Rodríguez-Santana A., Hernández-Guerra A., et al. 2008. Distribution of water masses and diapycnal mixing in the Cape Verde Frontal Zone. Geophys. Res. Lett. 35: L07609.
https://doi.org/10.1029/2008GL033229

Meyers S.D., Kelly B.G., O'Brien J.J. 1993. An Introduction to Wavelet Analysis in Oceanography and Meteorology: With Application to the Dispersion of Yanai Waves. Mon. Weather Rev. 121: 2858–2866.
https://doi.org/10.1175/1520-0493(1993)121<2858:AITWAI>2.0.CO;2

Mittelstaedt E. 1983. The upwelling area off Northwest Africa—A description of phenomena related to coastal upwelling. Prog. Oceanogr. 12: 307-331.
https://doi.org/10.1016/0079-6611(83)90012-5

Morlet J. 1983. Sampling Theory and Wave Propagation. In: Chen C.H. (ed), Issues in Acoustic Signal–Image Processing and Recognition. NATO ASI Series, vol 1. Springer, Berlin, Heidelberg, pp. 233-261.
https://doi.org/10.1007/978-3-642-82002-1_12

Morlet J., Arens G., Fourgeau E., et al. 1982. Wave propagation and sampling theory-Part I: Complex signal and scattering in multilayered media. Geophysics. 47: 203-221.
https://doi.org/10.1190/1.1441328

Moron V., Vautard R., Ghil M. 1998. Trends, interdecadal and interannual oscillations in global sea-surface temperatures. Clim. Dyn. 14: 545-569.
https://doi.org/10.1007/s003820050241

Navarro L., Martínez-Marrero A., Rodríguez-Santana A. 2018. Hydrographical and dynamical properties of the Cape Verde Frontal Zone during the FLUXES-II survey. Final degree project. Universidad de Las Palmas de Gran Canaria, 31 pp.

Pelegrí J.L., Peña-Izquierdo J., Machín F., et a. 2017. Deep-Sea Ecosystems Off Mauritania. In: Ramos A., Ramil F., Sanz J.L. (eds), Deep-Sea Ecosystems Off Mauritania. Springer Netherlands, pp. 119-153.
https://doi.org/10.1007/978-94-024-1023-5_3

Pérez F.F., Mintrop L., Llinás O., et al. 2001. Mixing analysis of nutrients, oxygen and inorganic carbon in the Canary Islands region. J. Mar. Syst. 28: 183-201.
https://doi.org/10.1016/S0924-7963(01)00003-3

Pérez-Rodríguez P., Pelegrí J.L., Marrero-Díaz A. 2001. Dynamical characteristics of the Cape Verde frontal zone. Sci. Mar. 65: 241-250.
https://doi.org/10.3989/scimar.2001.65s1241

Pollard R. 1986. Frontal surveys with a towed profiling conductivity/temperature/depth measurement package (SeaSoar). Nature 323: 433-435.
https://doi.org/10.1038/323433a0

Ramos A.G., García-Garrido V.J., Mancho A.M., et al. 2018. Lagrangian coherent structure assisted path planning for transoceanic autonomous underwater vehicle missions. Sci. Rep. 8: 4575.
https://doi.org/10.1038/s41598-018-23028-8

Rudnick D.L., Davis R.E., Eriksen C.C., et al. 2004. Underwater Gliders for Ocean Research. Mar. Technol. Soc. J. 38: 73-84
https://doi.org/10.4031/002533204787522703

von Schuckmann K., Le-Traon P.Y., Alvarez-Fanjul E., et al. 2016. The Copernicus Marine Environment Monitoring Service Ocean State Report. J. Oper. Oceanogr. 9: s235-s320.
https://doi.org/10.1080/1755876X.2016.1273446

Tomczak M. 1981. An analysis of mixing in the frontal zone of South and North Atlantic Central Water off North-West Africa. Prog. Oceanogr. 10: 173-192.
https://doi.org/10.1016/0079-6611(81)90011-2

Tomczak M., Hughes P. 1980. Three dimensional variability of water masses and currents in the Canary Current upwelling region. Meteor Forschungsergebnisse: Reihe A, Allgemeines, Physik und Chemie des Meeres. 21: 1-24.

Torrence C., Compo G.P. 1998. A Practical Guide to Wavelet Analysis. Bull. Am. Meteorol. Soc. 79: 61–78.
https://doi.org/10.1175/1520-0477(1998)079<0061:APGTWA>2.0.CO;2

Troupin C., Beltran J., Heslop E., et al. 2015. A toolbox for glider data processing and management. Methods in Oceanography. 13-14: 13-23.
https://doi.org/10.1016/j.mio.2016.01.001

Venkata-Ramana R., Krishna B., Kumar S.R., et al. 2013. Monthly Rainfall Prediction Using Wavelet Neural Network Analysis. Water Resour. Manage. 27: 3697-3711.
https://doi.org/10.1007/s11269-013-0374-4

Wang B., Wang Y. 1996. Temporal Structure of the Southern Oscillation as Revealed by Waveform and Wavelet Analysis. J. Clim. 9: 1586–1598.
https://doi.org/10.1175/1520-0442(1996)009<1586:TSOTSO>2.0.CO;2

Weng H., Lau K.M. 1994. Wavelets, Period Doubling, and Time-Frequency Localization with Application to Organization of Convection over the Tropical Western Pacific. J. Atmos. Sci. 51: 2523–2541.
https://doi.org/10.1175/1520-0469(1994)051<2523:WPDATL>2.0.CO;2

Yiou P., Sornette D., Ghil M. 2000. Data-adaptive wavelets and multiscale singular-spectrum analysis. Physica D. 142: 254-290.
https://doi.org/10.1016/S0167-2789(00)00045-2

Zenk W., Klein B., Schroder M. 1991. Cape Verde Frontal Zone. Deep Sea Res. Part. A. 38: S505-S530.
https://doi.org/10.1016/S0198-0149(12)80022-7